NASA TM X-371

NASA TM X-371

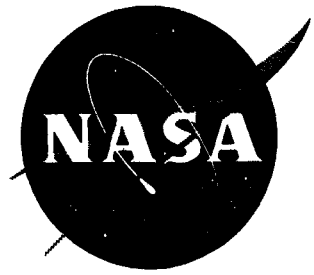

TECHNICAL MEMORANDUM

X-371

LIFT-DRAG RATIOS FOR ARROW WINGS ALONE AND IN COMBINATION WITH A BODY, NACELLES, AND VERTICAL TAILS AT MACH NUMBER 3

By William A. Hill, Jr.

Ames Research Center
Moffett Field, Calif.

NATIONAL AERONAUTICS AND SPACE ADMINISTRATION

WASHINGTON June 1960

NATIONAL AERONAUTICS AND SPACE ADMINISTRATION

TECHNICAL MEMORANDUM X-371

LIFT-DRAG RATIOS FOR ARROW WINGS ALONE AND IN COMBINATION WITH A BODY, NACELLES, AND VERTICAL TAILS AT MACH NUMBER 3*

By William A. Hill, Jr.

SUMMARY

Longitudinal and directional characteristics of cambered and twisted arrow wings alone and in combination with a slender body, vertical tails, and various arrangements of engine nacelles were measured for a Mach number of 2.94 and a Reynolds number of 3.5×10^6 (based on wing mean aerodynamic chord). The wing thickness-to-chord ratios were 2.1, 3.2, and 4.3 percent. The longitudinal characteristics of the 3.2-percent-thick wing were also measured at a Mach number of 0.2 and a Reynolds number of 6×10^6.

The highest maximum lift-drag ratio measured for the wings alone at a Mach number of 2.94 was 8.9. This value was obtained for the wings of thickness ratio 2.1 and 3.2 percent. Addition of the body to these wings resulted in a reduction in maximum lift-drag ratio from 8.9 to 7.3. Vertical tails attached to the tips of the 3.2-percent-thick wing provided the wing-body combination with directional stability but reduced the maximum lift-drag ratio from 7.3 to 7.1. The highest maximum lift-drag ratio obtained with nacelles added to the wing-body-tail combination was 6.8 for the model at trim. At a Mach number of 0.2, the 3.2-percent-thick wing had only moderate instability at high lift coefficients for a moment reference corresponding to that required for trim at a Mach number of 2.94.

INTRODUCTION

Recent interest in developing airplanes with high lift-drag ratios at Mach numbers near 3 has led to studies of arrow wings and of airplane configurations employing arrow wings (refs. 1 through 8). One arrow wing investigated in reference 2 was found to have a relatively high maximum lift-drag ratio (about 9) at a Mach number of 3 and a Reynolds number of 3.5×10^6. The wing, with leading edges swept 80°, was cambered and twisted in order to achieve a low drag due to lift and to trim at optimum lift

*Title, Unclassified

coefficient. Effects of changes in Reynolds number and supersonic Mach number on the lift-drag ratio of the wing were reported in reference 7. The effects of adding body volume to the wing in the form of bodies of both circular and elliptical cross section were studied in reference 8.

The primary purpose of the present investigation was to determine, at Mach number 3, the effects on lift-drag ratio and static stability of adding vertical tails and nacelles to this wing in combination with a body of high fineness ratio. Another purpose was to investigate the effects of changes in the wing thickness ratio, camber, and twist for wings alone and for wing-body combinations. A third purpose was to investigate the longitudinal stability characteristics of the wing alone at Mach number 0.2.

SYMBOLS

b span of wing-body combination with clipped wing tips (see fig. 1)

C_D drag coefficient, $\frac{D}{q_\infty S}$

C_L lift coefficient, $\frac{L}{q_\infty S}$

$C_{L_{opt}}$ lift coefficient at $\left(\frac{L}{D}\right)_{max}$

C_m pitching-moment coefficient about moment reference center shown in figure 1, $\frac{\text{pitching moment}}{q_\infty S\bar{c}}$

C_n yawing-moment coefficient about moment reference center shown in figure 1, $\frac{\text{yawing moment}}{q_\infty Sb}$

C_{n_β} $\left(\frac{\partial C_n}{\partial \beta}\right)_{\substack{\beta = 0 \\ \alpha = 0}}$, per radian

C_Y side-force coefficient, $\frac{\text{side force}}{q_\infty S}$

C_{Y_β} $\left(\frac{\partial C_Y}{\partial \beta}\right)_{\substack{\beta = 0 \\ \alpha = 0}}$, per radian

c root chord of exposed wing

c_o local chord of exposed wing

$\bar{c}$ mean aerodynamic chord of exposed wing

D drag (exclusive of base drag and internal drag)

d body base diameter

L lift

l body length (equal to 2c)

l_N body nose length

M_∞ free-stream Mach number

q_∞ free-stream dynamic pressure

r_N, x_N coordinates of body nose (see fig. 1(b))

S exposed wing plan-form area

t_{max} wing local maximum thickness

x, z Cartesian coordinates, x axis coincident with body longitudinal axis and lower surface of wing at root section, and z axis perpendicular to x axis in pitch plane

x_p distance from leading edge of wing root chord to center of pressure

x_r distance from leading edge of wing root chord to moment reference center (see fig. 1(b))

α angle of attack

α_{opt} angle of attack at $\left(\frac{L}{D}\right)_{max}$

β angle of sideslip

ϵ semiapex angle of wing leading edge

$\Delta(\ )$ incremental coefficient due to the addition of vertical tails or nacelles

Subscripts

L lower contour of wing section

max maximum

min minimum

U upper contour of wing section

MODELS AND TESTS

Models

Three arrow wings of essentially the same plan form (fig. 1(a)), but of different thickness-to-chord ratio, camber, and twist, were investigated at $M_\infty = 2.94$. The wings were designated as W_1, W_2, and W_3. Wing W_2 was model 6 of reference 2 and model W of reference 8, except that the tips were clipped as shown. (Clipping the tips was found to reduce $(L/D)_{max}$ by approximately 0.1.) This wing, previous to being twisted, had a Clark-Y airfoil (12 percent thick) normal to the leading edge. The section ordinates of W_1 and W_3 were obtained by the multiplication of the section ordinates of W_2 (untwisted) by 2/3 and 4/3, respectively. The resulting thickness-to-chord ratios of streamwise sections of wings W_1, W_2, and W_3 were 2.1, 3.2, and 4.3 percent, respectively. The ordinates of W_2 were referenced to the flat part of the lower surface of the airfoil rather than to the mean line. Thus, a change in section thickness was accompanied by a change in section camber. The wings were twisted by bending the wing tips upward about the axis shown, thereby decreasing the angle of attack of the tip sections relative to those at the root. The wings are defined in figure 1(a) by tabulated ordinates describing the wing bend, together with ordinates of streamwise sections of the untwisted wings. Ordinates for the bend are presented in terms of the displacement of the lower surface of the wing tip from the lower surface reference of the unbent wing. These ordinates are presented for the no-load condition and the test conditions for optimum lift coefficient ($\alpha \approx 4.5^\circ$). An 8-to-1 scale model of wing W_2 was tested at $M_\infty = 0.2$. This model is shown in figure 1(a) of reference 7.

The wings were constructed so that they could be tested alone or in combination with a body, B. It should be noted that the wings were parted at the root chord and mounted on the body so that their span was greater when tested in combination with the body. They were positioned so that the lower reference surface of the wings coincided with the midplane of the body. Body B was circular in cross section and consisted of a 3/4-power nose ($2r_N/d = (x_N/l_N)^{3/4}$) of fineness ratio 6 attached to a cylindrical afterbody 12.7 diameters long. The total volume of the models relative to the total plan area is tabulated in figure 1(b) in terms of the volume parameter, $(\text{volume}^{2/3})/(\text{plan area})$.

The tails, T, employed to provide directional stability to body-wing combination BW_2, were mounted on the wing tips (see fig. 1(b)). These tails were flat plates of arrow plan form and were 2.9 percent thick along the mean aerodynamic chord.

Four nacelle arrangements, designated as N_1, N_2, N_3, and N_4 in figure 1(b), were investigated to simulate engine installations for model BW_2T. For arrangements N_1, N_2, and N_3, two nacelles were attached beneath the wing and close to the body to simulate engine packs. Arrangement N_4 consisted of six smaller nacelles attached beneath the wing to simulate single-engine pods. All of the nacelles were straight-through ducts of circular cross section. Each nacelle arrangement had essentially the same total plan area, wetted area, and inlet area. The ratio of total inlet area to wing plan area was 0.010. A photograph of model BW_2TN_2 is presented in figure 1(c). All of the models were constructed of steel and were supported from the rear by stings attached to a strain-gage balance.

Tests

The tests at Mach number 2.94 were conducted in the Ames 1- by 3-Foot Supersonic Wind Tunnel No. 1. The Reynolds number, based on the wing mean aerodynamic chord, was 3.5 million. Lift, drag, and pitching moment were measured for all the models at zero sideslip and angles of attack from -7° to 6.4°. Side-force and yawing-moment measurements were obtained for complete configurations BW_2TN_1, BW_2TN_2, BW_2TN_3, and BW_2TN_4, and configurations BW_2T and BW_2 at zero angle of attack and angles of sideslip from 0° to 6°. Static pressures at the base of the support sting of the wings alone and at the base of the body were measured. No measurements were made of nacelle base pressure; however, base pressure estimates were obtained from reference 9. Visual-flow studies were made using the sublimation technique (see ref. 10) to determine the position of boundary-layer transition on the models.

The test at Mach number 0.2 was made in the Ames 12-foot pressure tunnel. The Reynolds number, based on the wing mean aerodynamic chord,

was 6 million. Lift, drag, and pitching moment were measured for the large-scale model of wing W_2 at zero sideslip and angles of attack from 0° to about 30°. Static pressures at the base of the support sting were recorded.

REDUCTION AND ACCURACY OF DATA

The force and moment data have been reduced to coefficient form based on the plan area and the mean aerodynamic chord of the wings. Pitching-moment coefficients are referred to the moment reference centers tabulated in figure 1(b). These locations were selected so that each model was trimmed at its optimum lift coefficient. To obtain the drag of the wings alone at $M_\infty = 2.94$, the measured drag of the support sting (which was tested without a wing attached) has been subtracted from the total measured drag. For the wing tested at $M_\infty = 0.2$ (wing W_2), the drag has been corrected for effects of tunnel wall interference; however, no adjustments in these data were made for the sting drag or the influence of the sting pressure field but these effects are believed to be small. The drag coefficients for the wings in combination with the body and nacelles ($M_\infty = 2.94$) have been adjusted to a condition of free-stream static pressure at the bases of the body and nacelles. For the models with nacelles, the internal drag of the nacelles has been subtracted from the total drag. The internal drag was assumed to result only from skin friction and was calculated for turbulent boundary-layer flow by the T' method of Rubesin and Johnson, as presented in reference 11.

The accuracy of the force and moment coefficients was determined from estimated uncertainties in the measurements of the forces and moments, dynamic pressures, and base pressures. The total uncertainties in the data are as follows:

	$M_\infty = 2.94$	$M_\infty = 0.2$
C_L	±0.002	±0.003
C_D	±.0002	±.0006
L/D	±.15	---
C_m	±.002	±.004
x_p/l	±.02	±.004
C_Y	±.002	---
C_n	±.002	---
M_∞	±.02	±.02
α	±.1	±.1
β	±.1	±.1

RESULTS AND DISCUSSION

Results from sublimation tests indicated that the boundary-layer flow over the models was turbulent except for a narrow region near the wing leading edges and a region near the body vertex. The results presented are, therefore, applicable for the case of turbulent boundary-layer flow on the models.

Longitudinal aerodynamic characteristics of wings W_1, W_2, and W_3 and body-wing combinations BW_1, BW_2, and BW_3 at zero angle of sideslip are presented in figures 2, 3, and 4. Longitudinal characteristics at zero angle of sideslip and directional characteristics at zero angle of attack for configurations B, W_2, BW_2, BW_2T, and BW_2TN_2 are presented in figures 5 and 6. Table I summarizes these experimental results together with results for configurations BW_2TN_1, BW_2TN_3, and BW_2TN_4. Also presented in table I are comparisons of estimated with experimental values of the incremental coefficients due to adding tails and nacelles to BW_2. The methods which were used for the estimates are designated at the bottom of table I. Comparisons of theory with experiment are omitted for the body-wing combinations. However, methods for computing the aerodynamic characteristics of arrow-wing and body combinations, and comparisons of theory with experiment for configurations similar to those of the present investigation are presented in reference 8.

Wings and Wing-Body Combinations

Comparison of the drag polars of the wings alone (fig. 2(b)) shows that the minimum drag coefficient was least for wing W_1, the thinnest wing, and increased with an increase in wing thickness, camber, and twist, as might be expected. However, the drag due to lift, $C_D - C_{D_{min}}$, at a given positive lift coefficient decreased slightly with increase in thickness, camber, and twist. As a result of these compensating effects, the maximum lift-drag ratios were about 8.9 for both wings W_1 and W_2 and 8.2 for wing W_3. Addition of the body to the wings substantially reduced the maximum lift-drag ratios. The maximum lift-drag ratios were about 7.3 for BW_1 and BW_2 and 7.0 for BW_3. As can be seen from figures 2 and 4, at the lift-drag ratios quoted the models are at trim and about neutrally stable.

A study of the above results indicates that a slight improvement in maximum lift-drag ratio might be realized by using a wing of the same thickness ratio as W_1 and the same camber as W_2. This can be reasoned by the fact that the minimum drag of W_1 was less than that of W_2, and the drag due to lift of W_2 was less than that of W_1.

The longitudinal characteristics of wing W_2 at $M_\infty = 0.2$ are compared in figure 3 with corresponding data for this wing at $M_\infty = 2.94$. It is

seen from the pitching-moment data for $M_\infty = 0.2$ (fig. 3(c)) that there was only moderate instability, at high lift coefficients, for a moment-reference location corresponding to that required for trim at $M_\infty = 2.94$. Similar results are shown in references 4 and 12 for an arrow wing with 75° swept leading edges tested at $M_\infty = 0.13$ and 2.87. However, from reference 12 it is indicated that instability at $M_\infty = 0.13$ can be reduced by the addition of wing-tip fins and virtually eliminated by the use of large fences along the wing upper surface. It is reasonable to assume that similar techniques could be employed to improve the stability of the present model (wing W_2) at $M_\infty = 0.2$.

Effects of Vertical Tails

Comparison of yawing-moment data for models BW_2 and BW_2T (fig. 6) shows that the wing-body combination (BW_2) became directionally stable with the addition of the vertical tails to the tips of the wing. However, addition of the tails also increased the minimum drag coefficient of the combination by about 6 percent (fig. 5(b)), and decreased $(L/D)_{max}$ from 7.3 to 7.1 (fig. 5(c)). Theoretical estimates of the tail-drag increment (principally turbulent skin-friction drag) and side-force and yawing-moment increments are shown in table I to be in good agreement with the experimental values.

Effects of Nacelles

Addition of the nacelles to BW_2T decreased $(L/D)_{max}$ by an additional 0.3 to 0.6, depending on nacelle arrangement (see table I). The highest $(L/D)_{max}$ measured for a complete configuration was 6.8 and was obtained by locating the nacelles near the wing-body juncture with the nacelle base in the plane of the body base (BW_2TN_2). The lowest value of $(L/D)_{max}$, 6.5, resulted when the nacelles were located beneath the body (BW_2TN_3). The effects of the nacelles on the longitudinal stability characteristics were negligible (see, e.g., fig. 5(d)).

The contribution of the nacelles to the directional characteristics of the complete configurations is indicated by the incremental side-force and yawing-moment derivatives presented in table I. The most effective arrangement for directional stability was N_3, in which case the nacelles, situated below the body, provided half the yawing-moment increment needed by model BW_2 for neutral directional stability. As shown in table I, the estimated increments of side force due to nacelles agree closely with the experimental increments for arrangements N_1, N_2, and N_4; whereas, for arrangement N_3, the estimated value is about one-half the experimental value. Comparison of yawing-moment increments shows fair agreement between experimental and estimated values.

SUMMARY OF RESULTS

Cambered and twisted arrow wings having thickness-to-chord ratios of 2.1, 3.2, and 4.3 percent were tested alone and in combination with a high-fineness-ratio body, vertical tails, and various arrangements of engine nacelles. The Mach number of the tests was 2.94, and the Reynolds number, based on wing mean aerodynamic chord, was 3.5×10^6. The 3.2-percent-thick wing was also tested at a Mach number of 0.2 and a Reynolds number of 6×10^6. The most significant results obtained are as follows:

1. The highest maximum lift-drag ratio measured for the wings alone at a Mach number of 2.94 was 8.9. This value was obtained for both the 2.1- and 3.2-percent-thick wings.

2. Addition of a high-fineness-ratio body to these wings resulted in a reduction in maximum lift-drag ratio from 8.9 to 7.3.

3. Addition of vertical tails provided directional stability but reduced the maximum lift-drag ratio from 7.3 to 7.1.

4. The highest maximum lift-drag ratio obtained for a combination of wing, body, tails, and nacelles was 6.8 for the model at trim.

5. At a Mach number of 0.2, the 3.2-percent-thick wing had only moderate longitudinal instability at high lift coefficients for a moment reference location corresponding to that required for trim at a Mach number of 2.94.

Ames Research Center
National Aeronautics and Space Administration
Moffett Field, Calif., Feb. 25, 1960

A 3 8 8

[redacted]

REFERENCES

1. Brown, Clinton E., and McLean, Francis E.: The Problem of Obtaining High Lift-Drag Ratios at Supersonic Speeds. I.A.S. Preprint No. 844, 1958.

2. Katzen, Elliott D.: Idealized Wings and Wing-Bodies at a Mach Number of 3. NACA TN 4361, 1958.

3. Mueller, James N., and Grimaud, John E.: Effects of Twist and Camber and Thickness on the Aerodynamic Characteristics of a 75° Swept Arrow Wing at a Mach Number of 2.91. NASA TM X-138, 1959.

4. Hallissy, Joseph M., Jr., and Hasson, Dennis F.: Aerodynamic Characteristics at Mach Numbers 2.36 and 2.87 of an Airplane Configuration Having a Cambered Arrow Wing With a 75° Swept Leading Edge. NACA RM L58E21, 1958.

5. Hasson, Dennis F., Fichter, Ann B., and Wong, Norman: Aerodynamic Characteristics at Mach Numbers From 1.6 to 2.8 of 74° Swept Arrow Wings With and Without Camber and Twist. NASA TM X-8, 1959.

6. Hasson, Dennis F., and Wong, Norman: Aerodynamic Characteristics at Mach Numbers From 2.29 to 4.65 of 80° Swept Arrow Wings With and Without Camber and Twist. NASA TM X-175, 1960.

7. Hopkins, Edward J., Jillie, Don W., and Levin, Alan D.: Lift, Drag, and Pitching Moments of an Arrow Wing Having 80° of Sweepback at Mach Numbers From 2.48 to 3.51 and Reynolds Numbers Up to 11.0 Million. NASA TM X-22, 1959.

8. Jorgensen, Leland H.: Lift-Drag Ratios for an Arrow Wing With Bodies at Mach Number 3. NASA MEMO 4-27-59A, 1959.

9. Hargis, Calvin B., Davison, P. H., and Savage, S. B.: Methods for Estimating Base Pressures on Aircraft Configurations. WADC Tech. Note 57-28, 1957.

10. Main-Smith, J. D.: Chemical Solids as Diffusible Coating Films for Visual Indications of Boundary-Layer Transition in Air and Water. British R & M No. 2755, 1950. (Brit. R.A.E. Chem. 466, Feb. 1950)

11. Sommer, Simon C., and Short, Barbara J.: Free-Flight Measurements of Turbulent-Boundary-Layer Skin Friction in the Presence of Severe Aerodynamic Heating at Mach Numbers From 2.8 to 7.0. NACA TN 3391, 1955.

A 3 8 8

[redacted]

12. Naeseth, Rodger L., and Davenport, Edwin E.: Low Speed Wind-Tunnel Investigation of the Aerodynamic Characteristics of an Airplane Having a Cambered Arrow Wing With a 75° Swept Leading Edge. NASA TM X-185, 1960.

13. Moskowitz, Barry: Approximate Theory for Calculation of Lift of Bodies, Afterbodies, and Combinations of Bodies. NACA TN 2669, 1952.

TABLE I.- SUMMARY OF RESULTS; $M_\infty = 2.94$

Configuration or component	$(L/D)_{max}$	$C_{D_{min}}$	$\Delta C_{D_{min}}$				$\frac{C_{L_{opt}}}{\alpha_{opt}}$ (1)	$\frac{\Delta C_{L_{opt}}}{\alpha_{opt}}$ (1)		C_{Y_β}	ΔC_{Y_β}		C_{n_β}	ΔC_{n_β} (2)	
	Experimental		Experimental	Estimated											
			Total	Total	Skin friction (3)	Wave (4)	Experimental	Experimental	Estimated (5)	Experimental	Experimental	Estimated (5)	Experimental	Experimental	Estimated (5)
B		0.0035													
W_1	8.9	.0044													
W_2	8.9	.0048													
W_3	8.2	.0055													
BW_1	7.3	.0079					1.31								
BW_2	7.3	.0083					1.31			-0.10			-0.07		
BW_3	7.0	.0090					1.28								
BW_2T	7.1	.0088					1.31			-.19			.05		
BW_2TN_1	6.6	.0099					1.42			-.24			.04		
BW_2TN_2	6.8	.0098					1.43			-.24			.05		
BW_2TN_3	6.5	.0101					1.37			-.30			.08		
BW_2TN_4	6.6	.0101					1.41			-.24			.07		
T			0.0005	0.0004	0.0003	0.0001		0	0		-0.09	-0.10		0.12	0.14
N_1			.0011	.0010	.0009	.0001		.11	.05		-.05	-.05		-.01	.01
N_2			.0010	.0010	.0009	.0001		.12	.05		-.05	-.05		0	.02
N_3			.0013	.0010	.0009	.0001		.06	.05		-.11	-.05		.03	.02
N_4			.0013	.0011	.0010	.0001		.10	.05		-.05	-.05		.02	.03

[1] $\alpha_{opt} \approx 0.081$ radian

[2] Referred to $\frac{x_r}{l} = 0.427$

[3] 'T' method for turbulent boundary layer (ref. 11)

[4] Tails - Newtonian theory; nacelles - linear theory

[5] Tails - Linear theory; nacelles - slender body theory (ref. 13)

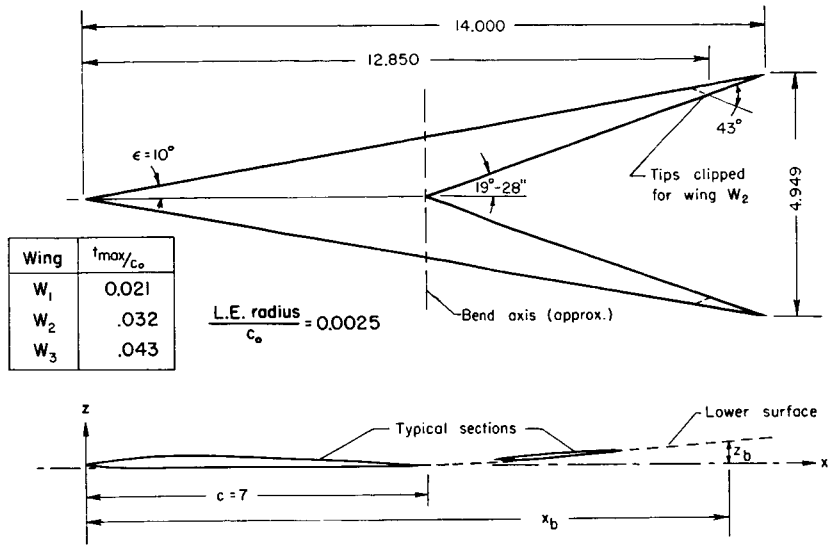

Wing	t_{max}/c_o
W_1	0.021
W_2	.032
W_3	.043

$\frac{\text{L.E. radius}}{c_o} = 0.0025$

Airfoil ordinates of untwisted wings

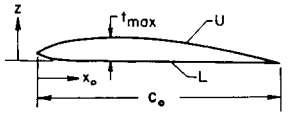

$\frac{x_o}{c_o}$	$\frac{z_U}{t_{max}}$	$\frac{z_L}{t_{max}}$
0	0.363	0.363
.05	.655	.168
.10	.787	.098
.15	.878	.058
.20	.937	.038
.25	.979	.022
.30	1.000	.012
.35	1.003	.003
.40	.992	0
.45	.969	
.50	.935	
.55	.890	
.60	.839	
.65	.774	
.70	.694	
.75	.598	
.80	.493	
.85	.377	
.90	.255	
.95	.128	
1.00	0	

Note: Linear dimensions in inches

Lower-surface ordinates of twisted wings

$\frac{x_b}{c}$	$\frac{z_b}{c}$					
	No load			$\frac{q_\infty}{M_\infty^2} \approx 160$ psf, $\alpha \approx 4.5°$		
	W_1	W_2	W_3	W_1	W_2	W_3
1.00	0	0	0	0	0	0
1.10	.003	.004	.004	.003	.004	.004
1.20	.007	.011	.011	.008	.011	.011
1.30	.012	.019	.020	.016	.022	.021
1.40	.016	.027	.030	.023	.031	.032
1.60	.026	.044	.052	.039	.051	.056
1.84	.037	.064	.078	.057	.073	.084
2.00	.045	—	.096	.070	—	.103

(a) Wing geometry.

Figure 1.- Models.

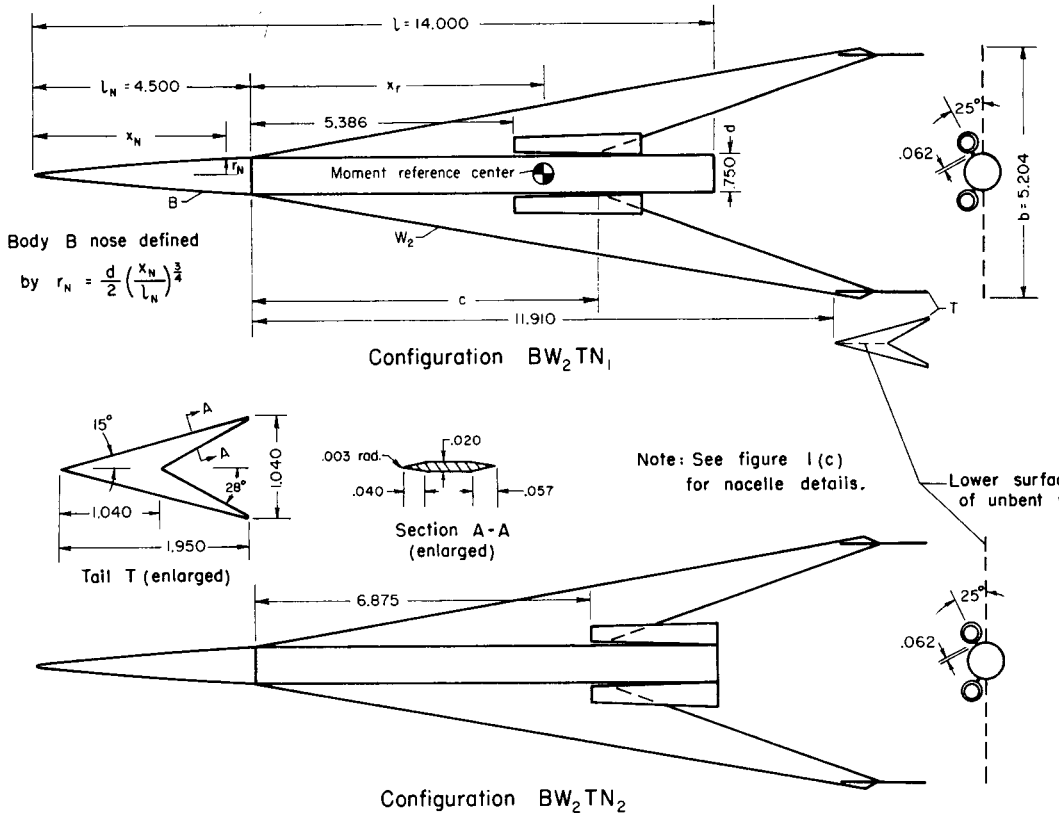

Model	$\frac{x_r}{l}$	$\frac{(\text{Total volume})^{\frac{2}{3}}}{\text{Total plan area}}$
B	0.410	1.155
W_1	.454	.066
W_2	.468	.086
W_3	.453	.105
BW_1	.404	.128
BW_2	.410	.137
BW_3	.404	.145
BW_2T	.418	.137
BW_2TN_1	.417	↓
BW_2TN_2	.428	
BW_2TN_3	.421	
BW_2TN_4	.425	

Note: Linear dimensions in inches

(b) Wing - body - tail - nacelle geometry.

Figure 1.- Continued.

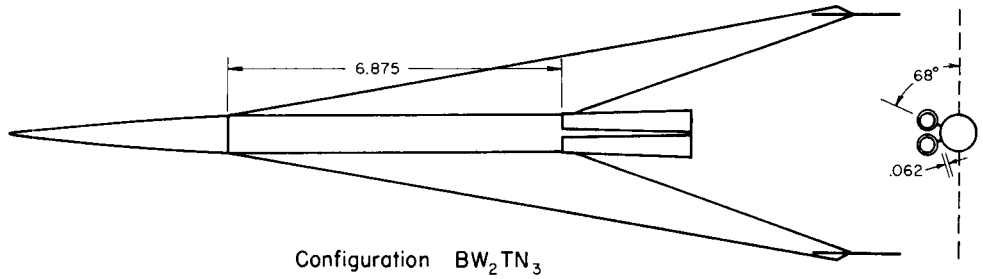

Configuration BW_2TN_3

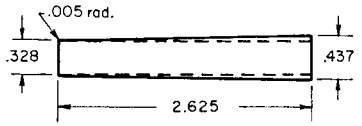

Nacelle (enlarged) for arrangements N_1, N_2, and N_3

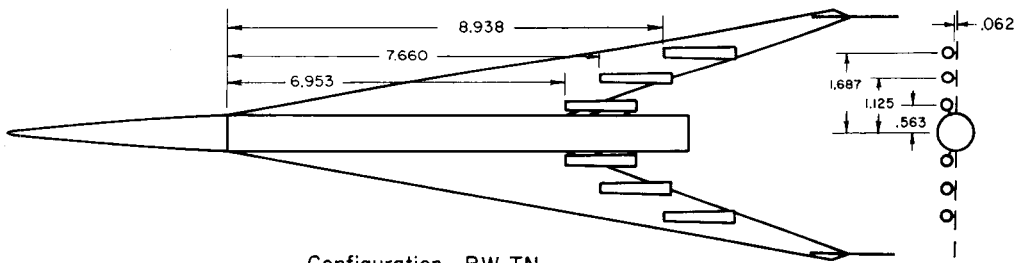

Configuration BW_2TN_4

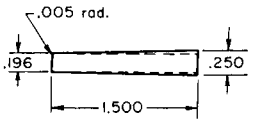

Nacelle (enlarged) for arrangement N_4

Note: Linear dimensions in inches

(b) Concluded.

Figure 1.- Continued.

A-25556

(c) Model BW_2TN_2.

Figure 1.- Concluded.

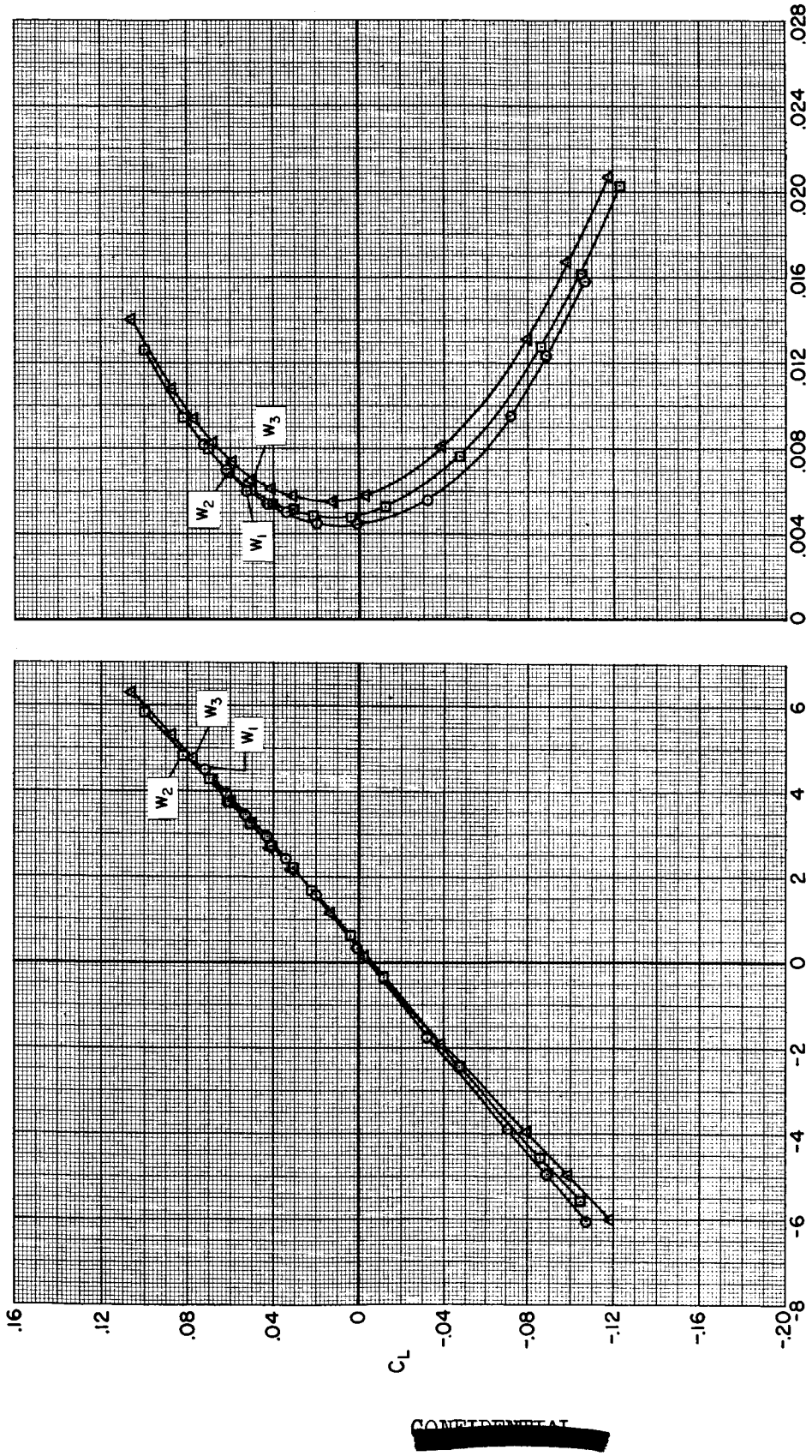

Figure 2.- Longitudinal aerodynamic characteristics of wings W_1, W_2, and W_3; $M_\infty = 2.94$; $\beta = 0^\circ$.

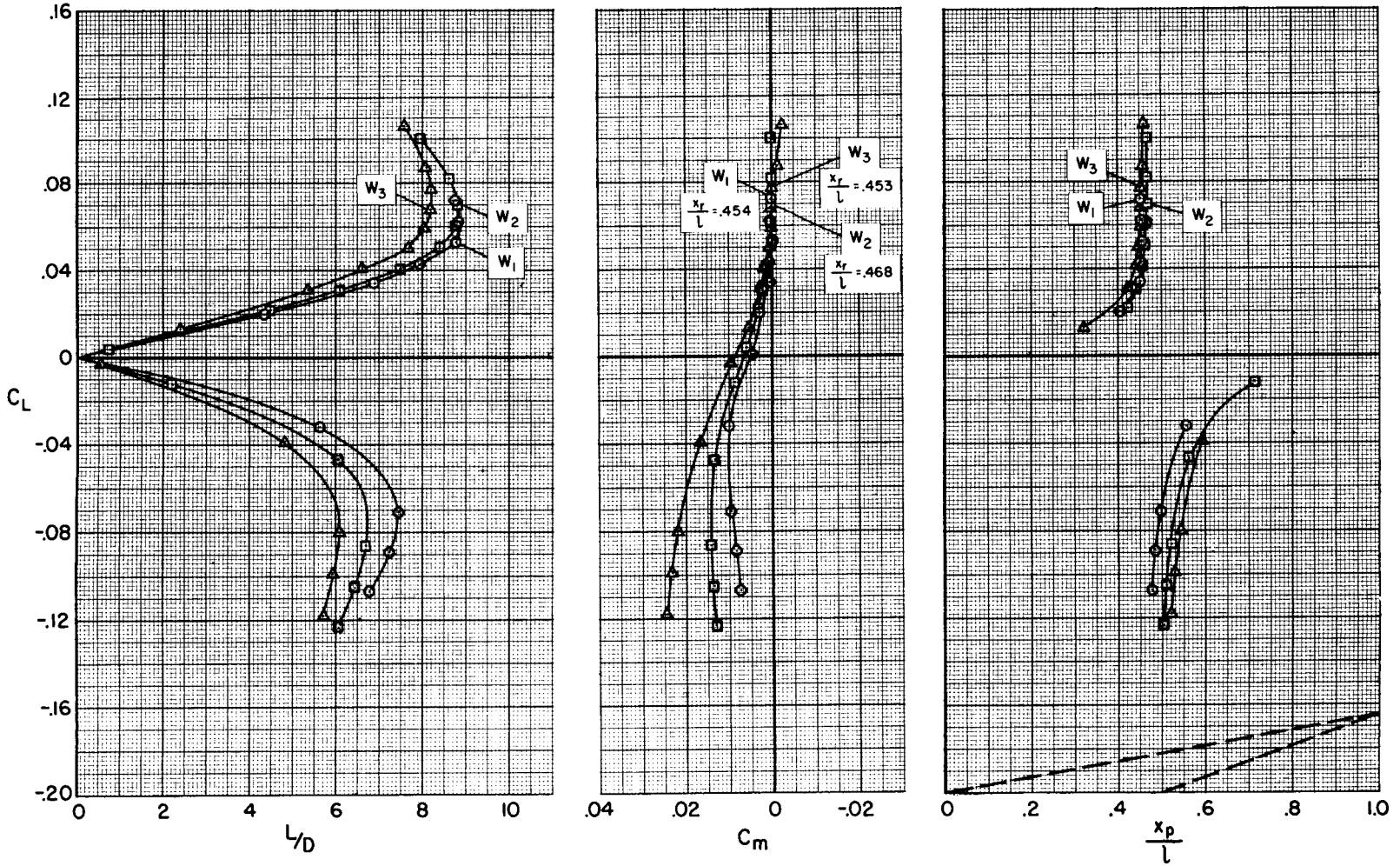

(c) Lift-drag ratio.

(d) Pitching moment.

(e) Center of pressure.

Figure 2.- Concluded.

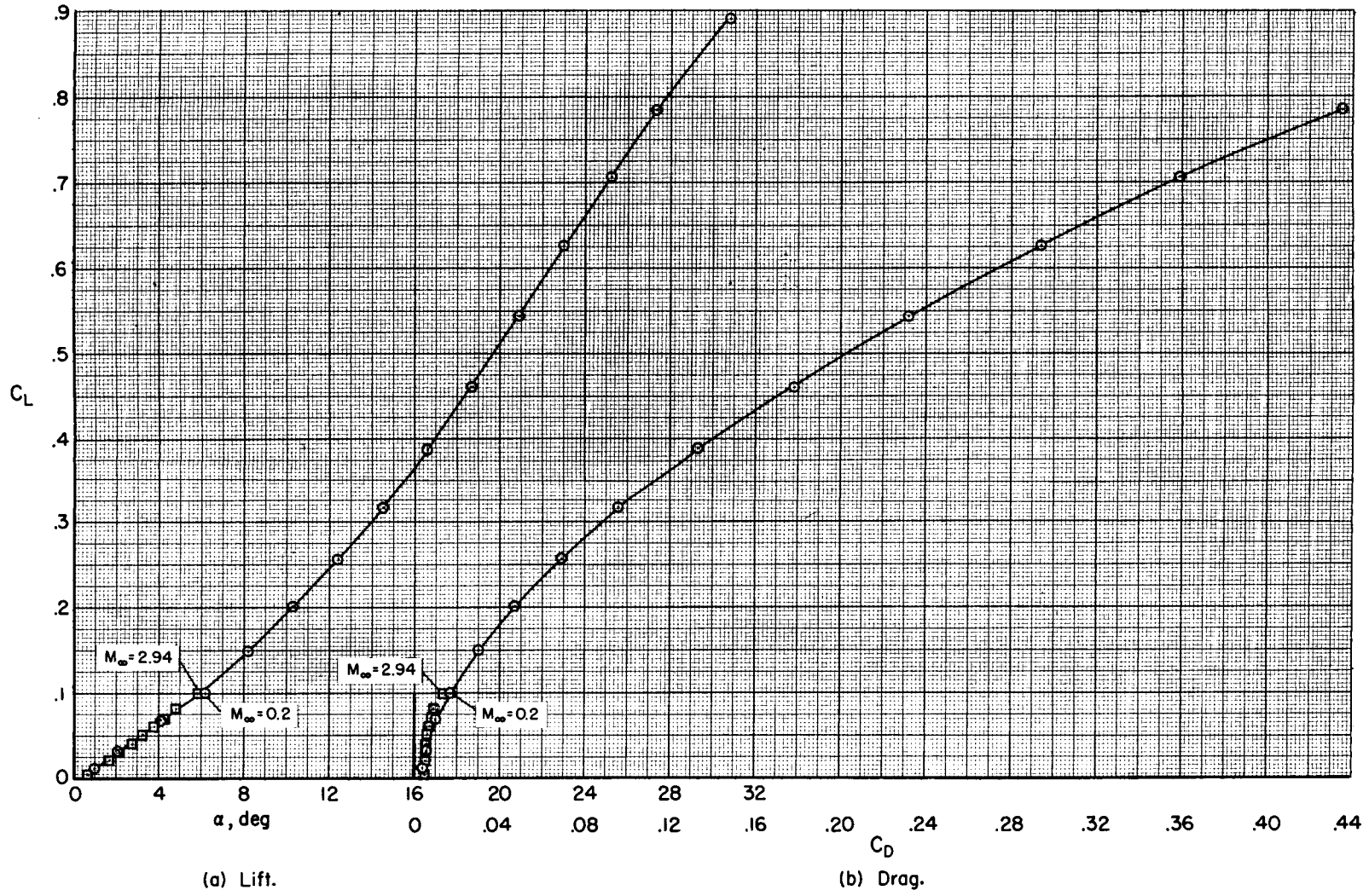

Figure 3.- Longitudinal aerodynamic characteristics of wing W_2 at $M_\infty = 0.2$ and 2.94; $\beta = 0^\circ$.

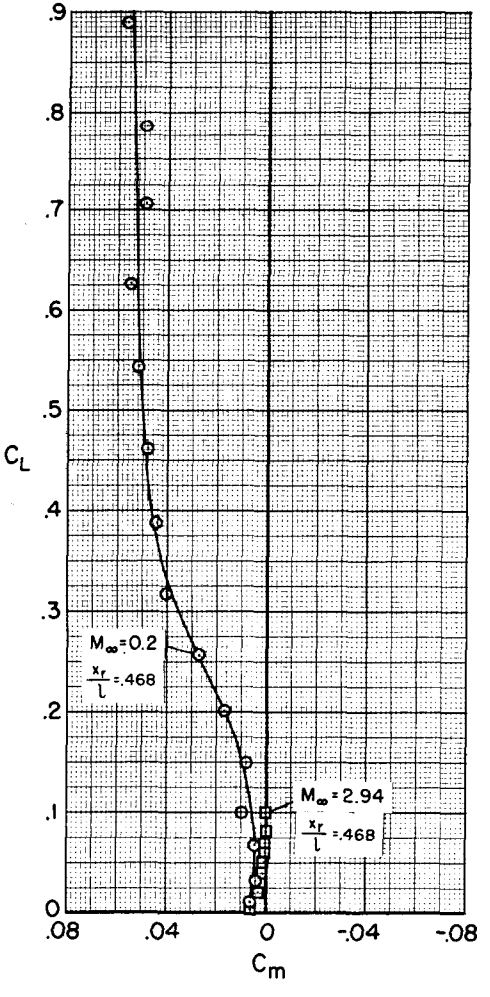

(c) Pitching moment.

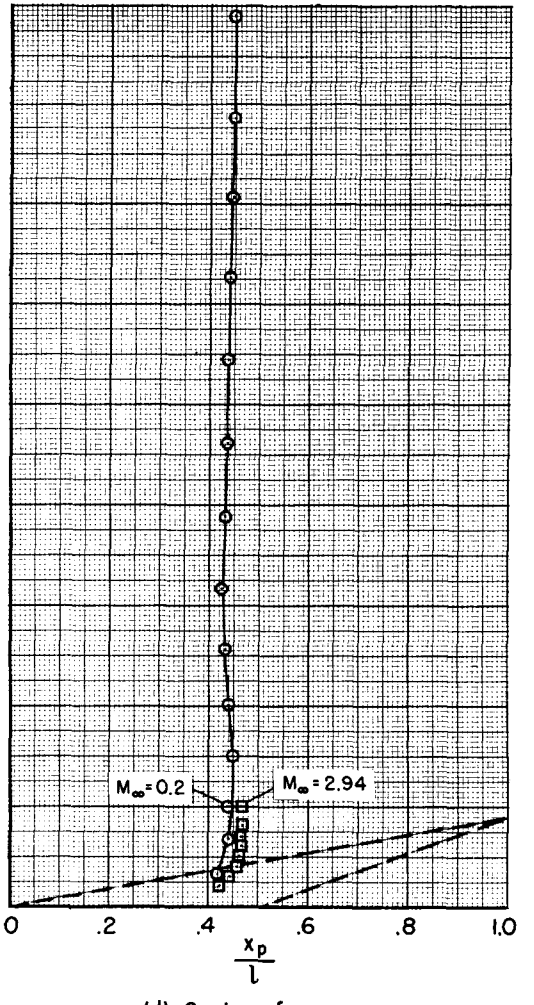

(d) Center of pressure.

Figure 3.- Concluded.

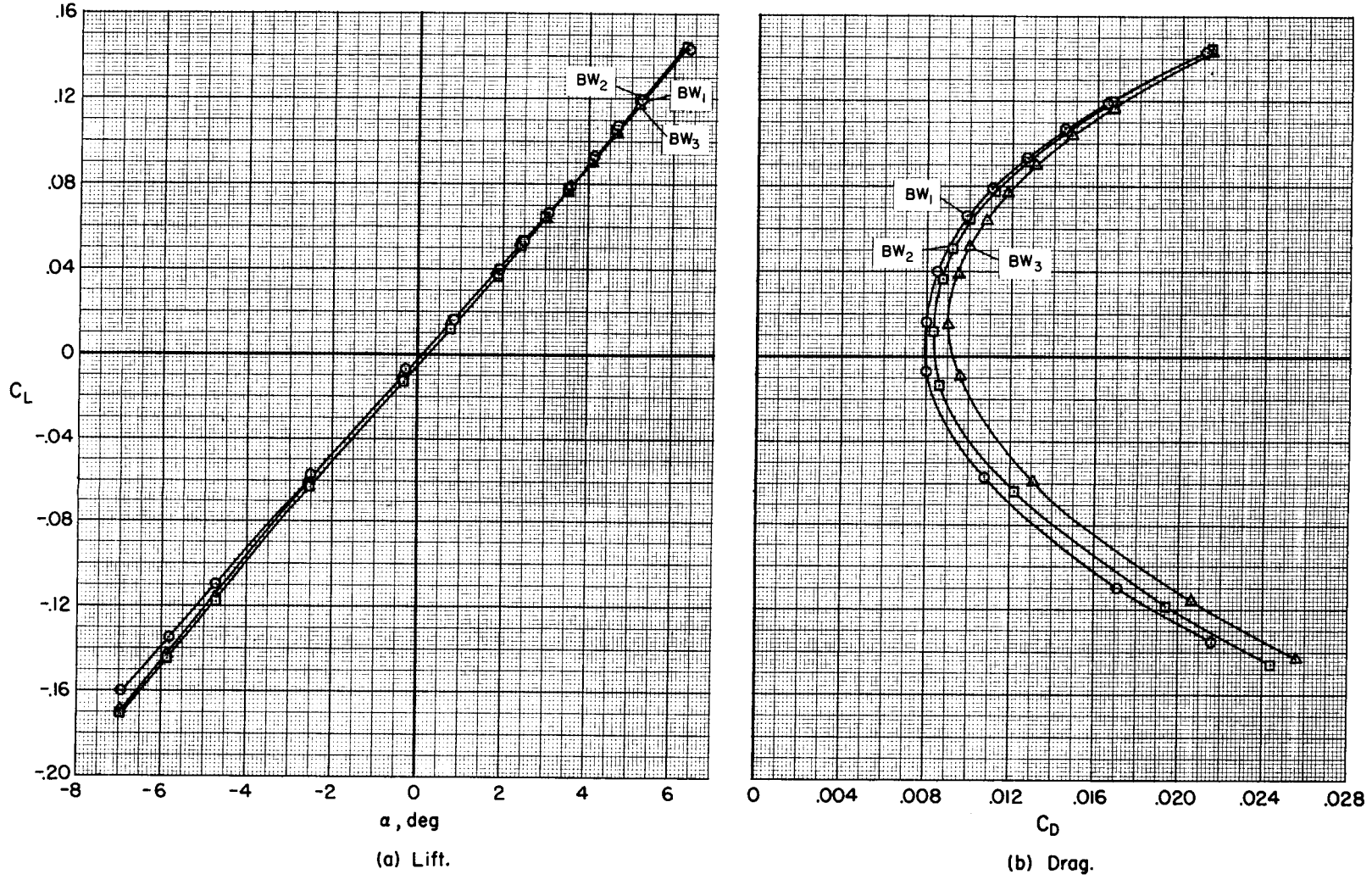

Figure 4.- Longitudinal aerodynamic characteristics of body-wing combinations BW_1, BW_2, and BW_3; $M_\infty = 2.94$; $\beta = 0^\circ$.

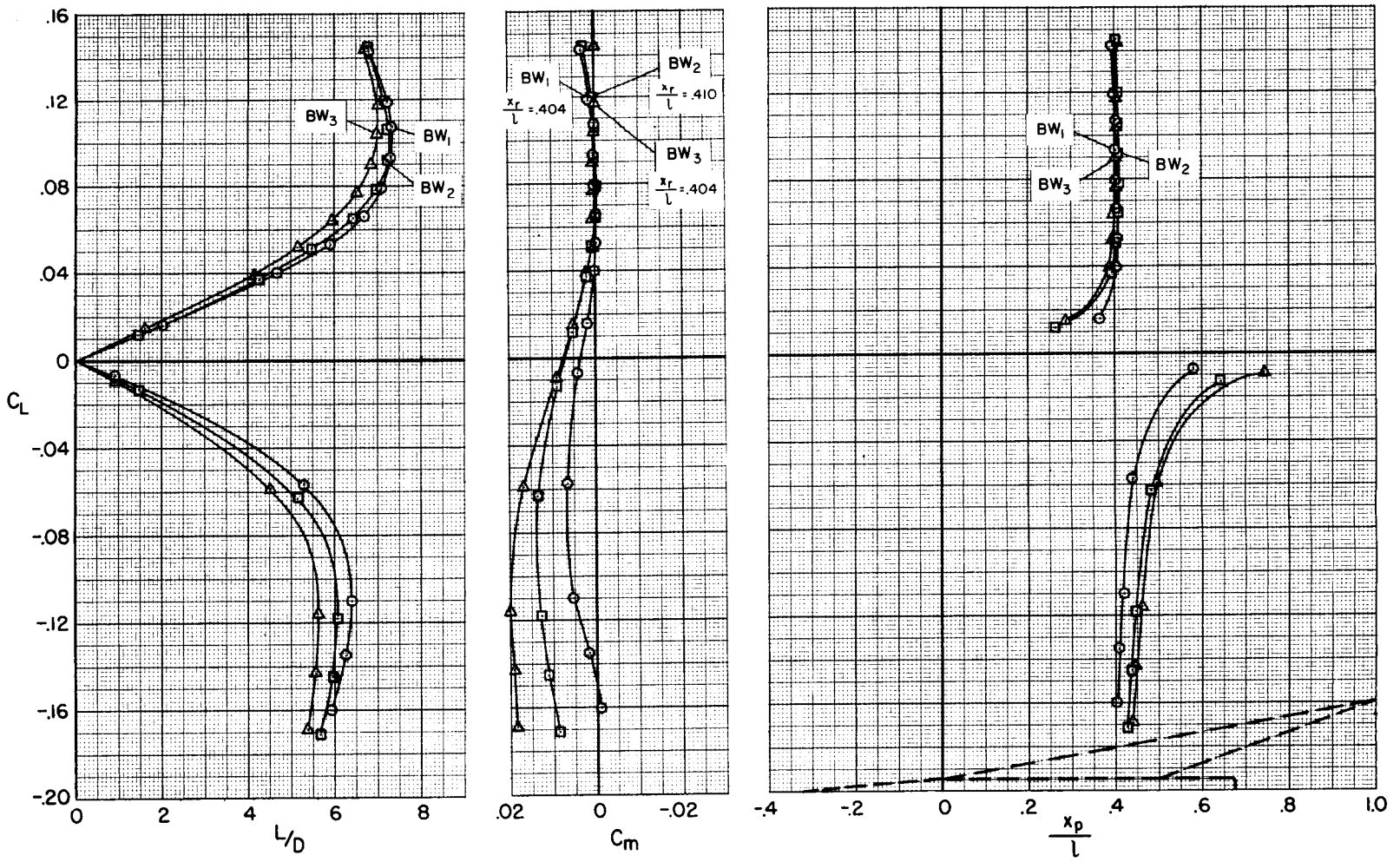

(c) Lift-drag ratio.

(d) Pitching moment.

(e) Center of pressure.

Figure 4.- Concluded.

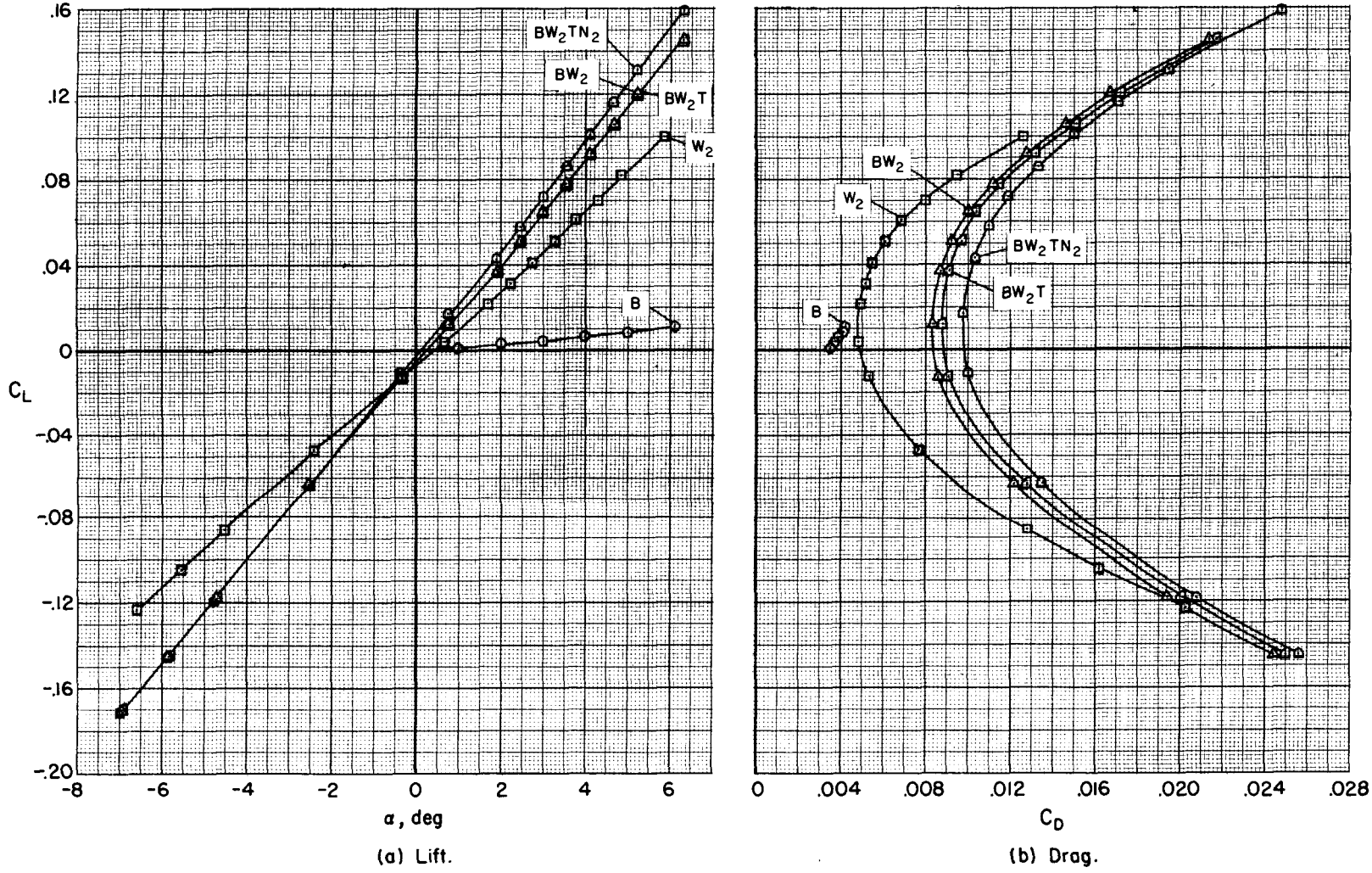

Figure 5.- Longitudinal aerodynamic characteristics of models B, W_2, BW_2, BW_2T, and BW_2TN_2; $M_\infty = 2.94$; $\beta = 0^\circ$.

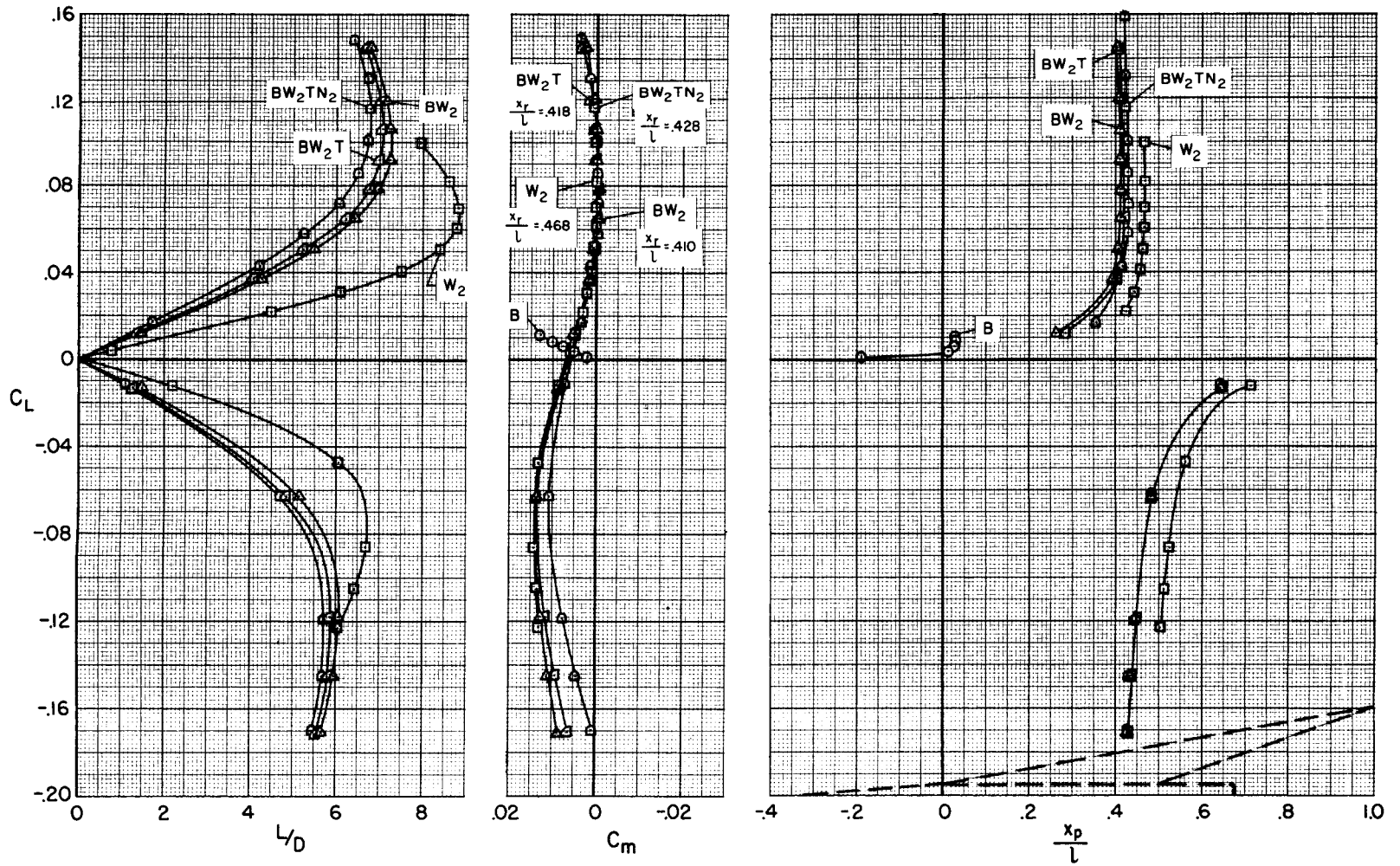

Figure 5.- Concluded.

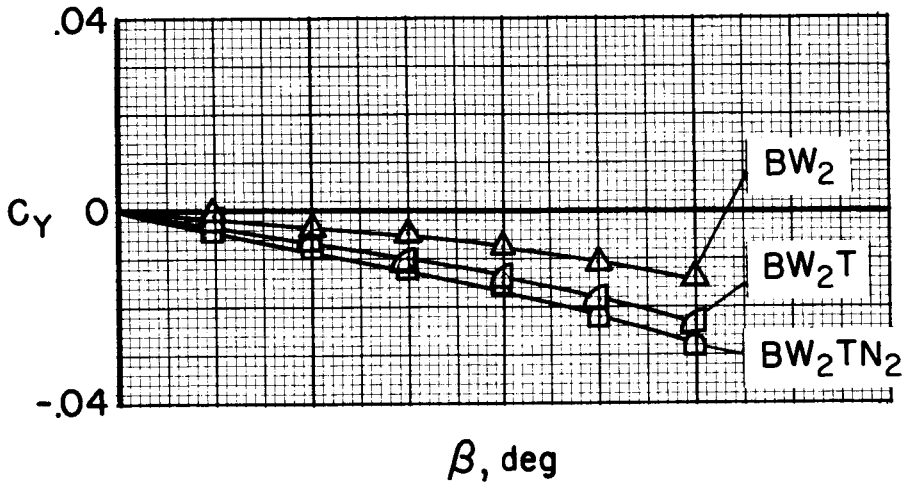

(a) Side force.

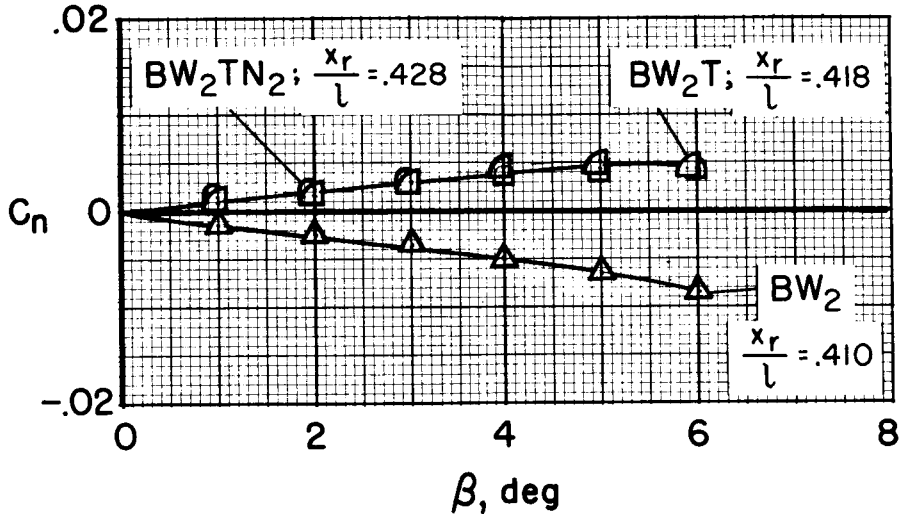

(b) Yawing moment.

Figure 6.- Directional aerodynamic characteristics of models BW_2, BW_2T, and BW_2TN_2; $M_\infty = 2.94$; $\alpha = 0^\circ$.